

Probing the gluonic structure of the deuteron with J/ψ photoproduction in d+Au ultra-peripheral collisions

M. S. Abdallah,⁵ B. E. Aboona,⁵⁵ J. Adam,⁶ L. Adamczyk,² J. R. Adams,³⁹ J. K. Adkins,³⁰ G. Agakishiev,²⁸
I. Aggarwal,⁴¹ M. M. Aggarwal,⁴¹ Z. Ahammed,⁶⁰ I. Alekseev,^{3,35} D. M. Anderson,⁵⁵ A. Aparin,²⁸
E. C. Aschenauer,⁶ M. U. Ashraf,¹¹ F. G. Atetalla,²⁹ A. Attri,⁴¹ G. S. Averichev,²⁸ V. Bairathi,⁵³ W. Baker,¹⁰
J. G. Ball Cap,²⁰ K. Barish,¹⁰ A. Behera,⁵² R. Bellwied,²⁰ P. Bhagat,²⁷ A. Bhasin,²⁷ J. Bielcik,¹⁴ J. Bielcikova,³⁸
I. G. Bordyuzhin,³ J. D. Brandenburg,⁶ A. V. Brandin,³⁵ I. Bunzarov,²⁸ X. Z. Cai,⁵⁰ H. Caines,⁶³
M. Calderón de la Barca Sánchez,⁸ D. Cebra,⁸ I. Chakaberia,^{31,6} P. Chaloupka,¹⁴ B. K. Chan,⁹ F-H. Chang,³⁷
Z. Chang,⁶ N. Chankova-Bunzarova,²⁸ A. Chatterjee,¹¹ S. Chattopadhyay,⁶⁰ D. Chen,¹⁰ J. Chen,⁴⁹ J. H. Chen,¹⁸
X. Chen,⁴⁸ Z. Chen,⁴⁹ J. Cheng,⁵⁷ M. Chevalier,¹⁰ S. Choudhury,¹⁸ W. Christie,⁶ X. Chu,⁶ H. J. Crawford,⁷
M. Csanád,¹⁶ M. Daugherty,¹ T. G. Dedovich,²⁸ I. M. Deppner,¹⁹ A. A. Derevschikov,⁴³ A. Dhamija,⁴¹
L. Di Carlo,⁶² L. Didenko,⁶ P. Dixit,²² X. Dong,³¹ J. L. Drachenberg,¹ E. Duckworth,²⁹ J. C. Dunlop,⁶ N. Elsey,⁶²
J. Engelage,⁷ G. Eppley,⁴⁵ S. Esumi,⁵⁸ O. Evdokimov,¹² A. Ewigleben,³² O. Eyser,⁶ R. Fatemi,³⁰ F. M. Fawzi,⁵
S. Fazio,⁶ P. Federic,³⁸ J. Fedorisin,²⁸ C. J. Feng,³⁷ Y. Feng,⁴⁴ P. Filip,²⁸ E. Finch,⁵¹ Y. Fisyak,⁶ A. Francisco,⁶³
C. Fu,¹¹ L. Fulek,² C. A. Gagliardi,⁵⁵ T. Galatyuk,¹⁵ F. Geurts,⁴⁵ N. Ghimire,⁵⁴ A. Gibson,⁵⁹ K. Gopal,²³
X. Gou,⁴⁹ D. Grosnick,⁵⁹ A. Gupta,²⁷ W. Guryn,⁶ A. I. Hamad,²⁹ A. Hamed,⁵ Y. Han,⁴⁵ S. Harabasz,¹⁵
M. D. Harasty,⁸ J. W. Harris,⁶³ H. Harrison,³⁰ S. He,¹¹ W. He,¹⁸ X. H. He,²⁶ Y. He,⁴⁹ S. Heppelmann,⁸
S. Heppelmann,⁴² N. Herrmann,¹⁹ E. Hoffman,²⁰ L. Holub,¹⁴ Y. Hu,¹⁸ H. Huang,³⁷ H. Z. Huang,⁹ S. L. Huang,⁵²
T. Huang,³⁷ X. Huang,⁵⁷ Y. Huang,⁵⁷ T. J. Humanic,³⁹ G. Igo,^{9,*} D. Isenhower,¹ W. W. Jacobs,²⁵ C. Jena,²³
A. Jentsch,⁶ Y. Ji,³¹ J. Jia,^{6,52} K. Jiang,⁴⁸ X. Ju,⁴⁸ E. G. Judd,⁷ S. Kabana,⁵³ M. L. Kabir,¹⁰ S. Kagamaster,³²
D. Kalinkin,^{25,6} K. Kang,⁵⁷ D. Kapukchyan,¹⁰ K. Kauder,⁶ H. W. Ke,⁶ D. Keane,²⁹ A. Kechechyan,²⁸ M. Kelsey,⁶²
Y. V. Khyzhniak,³⁵ D. P. Kikoła,⁶¹ C. Kim,¹⁰ B. Kimelman,⁸ D. Kincses,¹⁶ I. Kisel,¹⁷ A. Kiselev,⁶ A. G. Knospe,³²
H. S. Ko,³¹ L. Kochenda,³⁵ L. K. Kosarzewski,¹⁴ L. Kramarik,¹⁴ P. Kravtsov,³⁵ L. Kumar,⁴¹ S. Kumar,²⁶
R. Kunnawalkam Elayavalli,⁶³ J. H. Kwasizur,²⁵ R. Lacey,⁵² S. Lan,¹¹ J. M. Landgraf,⁶ J. Lauret,⁶ A. Lebedev,⁶
R. Lednicky,^{28,38} J. H. Lee,⁶ Y. H. Leung,³¹ C. Li,⁴⁹ C. Li,⁴⁸ W. Li,⁴⁵ X. Li,⁴⁸ Y. Li,⁵⁷ X. Liang,¹⁰ Y. Liang,²⁹
R. Licenik,³⁸ T. Lin,⁴⁹ Y. Lin,¹¹ M. A. Lisa,³⁹ F. Liu,¹¹ H. Liu,²⁵ H. Liu,¹¹ P. Liu,⁵² T. Liu,⁶³ X. Liu,³⁹ Y. Liu,⁵⁵
Z. Liu,⁴⁸ T. Ljubicic,⁶ W. J. Llope,⁶² R. S. Longacre,⁶ E. Loyd,¹⁰ N. S. Lukow,⁵⁴ X. F. Luo,¹¹ L. Ma,¹⁸ R. Ma,⁶
Y. G. Ma,¹⁸ N. Magdy,¹² D. Mallick,³⁶ S. Margetis,²⁹ C. Markert,⁵⁶ H. S. Matis,³¹ J. A. Mazer,⁴⁶ N. G. Minaev,⁴³
S. Mioduszewski,⁵⁵ B. Mohanty,³⁶ M. M. Mondal,⁵² I. Mooney,⁶² D. A. Morozov,⁴³ A. Mukherjee,¹⁶ M. Nagy,¹⁶
J. D. Nam,⁵⁴ Md. Nasim,²² K. Nayak,¹¹ D. Neff,⁹ J. M. Nelson,⁷ D. B. Nemes,⁶³ M. Nie,⁴⁹ G. Nigmatkulov,³⁵
T. Niida,⁵⁸ R. Nishitani,⁵⁸ L. V. Nogach,⁴³ T. Nonaka,⁵⁸ A. S. Nunes,⁶ G. Odyniec,³¹ A. Ogawa,⁶ S. Oh,³¹
V. A. Okorokov,³⁵ B. S. Page,⁶ R. Pak,⁶ J. Pan,⁵⁵ A. Pandav,³⁶ A. K. Pandey,⁵⁸ Y. Panebratsev,²⁸ P. Parfenov,³⁵
B. Pawlik,⁴⁰ D. Pawlowska,⁶¹ C. Perkins,⁷ L. Pinsky,²⁰ R. L. Pintér,¹⁶ J. Pluta,⁶¹ B. R. Pokhrel,⁵⁴
G. Pomatkin,³⁸ J. Porter,³¹ M. Posik,⁵⁴ V. Prozorova,¹⁴ N. K. Pruthi,⁴¹ M. Przybycien,² J. Putschke,⁶²
H. Qiu,²⁶ A. Quintero,⁵⁴ C. Racz,¹⁰ S. K. Radhakrishnan,²⁹ N. Raha,⁶² R. L. Ray,⁵⁶ R. Reed,³² H. G. Ritter,³¹
M. Robotkova,³⁸ O. V. Rogachevskiy,²⁸ J. L. Romero,⁸ D. Roy,⁴⁶ L. Ruan,⁶ J. Rusnak,³⁸ N. R. Sahoo,⁴⁹ H. Sako,⁵⁸
S. Salur,⁴⁶ J. Sandweiss,^{63,*} S. Sato,⁵⁸ W. B. Schmidke,⁶ N. Schmitz,³³ B. R. Schweid,⁵² F. Seck,¹⁵ J. Seger,¹³
M. Sergeeva,⁹ R. Seto,¹⁰ P. Seyboth,³³ N. Shah,²⁴ E. Shahaliev,²⁸ P. V. Shanmuganathan,⁶ M. Shao,⁴⁸ T. Shao,¹⁸
A. I. Sheikh,²⁹ D. Shen,⁵⁰ S. S. Shi,¹¹ Y. Shi,⁴⁹ Q. Y. Shou,¹⁸ E. P. Sichtermann,³¹ R. Sikora,² M. Simko,³⁸
J. Singh,⁴¹ S. Singha,²⁶ M. J. Skoby,⁴⁴ N. Smirnov,⁶³ Y. Söhnngen,¹⁹ W. Solyst,²⁵ P. Sorensen,⁶ H. M. Spinka,^{4,*}
B. Srivastava,⁴⁴ T. D. S. Stanislaus,⁵⁹ M. Stefaniak,⁶¹ D. J. Stewart,⁶³ M. Strikhanov,³⁵ B. Stringfellow,⁴⁴
A. A. P. Suaide,⁴⁷ M. Sumera,³⁸ B. Summa,⁴² X. M. Sun,¹¹ X. Sun,¹² Y. Sun,⁴⁸ Y. Sun,²¹ B. Surrow,⁵⁴
D. N. Svirida,³ Z. W. Sweger,⁸ P. Szymanski,⁶¹ A. H. Tang,⁶ Z. Tang,⁴⁸ A. Taranenko,³⁵ T. Tarnowsky,³⁴
J. H. Thomas,³¹ A. R. Timmins,²⁰ D. Tlusty,¹³ T. Todoroki,⁵⁸ M. Tokarev,²⁸ C. A. Tomkiel,³² S. Trentalange,⁹
R. E. Tribble,⁵⁵ P. Tribedy,⁶ S. K. Tripathy,¹⁶ T. Truhlar,¹⁴ B. A. Trzeciak,¹⁴ O. D. Tsai,⁹ Z. Tu,⁶ T. Ullrich,⁶
D. G. Underwood,^{4,59} I. Upsal,⁴⁵ G. Van Buren,⁶ J. Vanek,³⁸ A. N. Vasiliev,⁴³ I. Vassiliev,¹⁷ V. Verkest,⁶²
F. Videbæk,⁶ S. Vokal,²⁸ S. A. Voloshin,⁶² F. Wang,⁴⁴ G. Wang,⁹ J. S. Wang,²¹ P. Wang,⁴⁸ Y. Wang,¹¹ Y. Wang,⁵⁷
Z. Wang,⁴⁹ J. C. Webb,⁶ P. C. Weidenkaff,¹⁹ L. Wen,⁹ G. D. Westfall,³⁴ H. Wieman,³¹ S. W. Wissink,²⁵ J. Wu,²⁶
Y. Wu,¹⁰ B. Xi,⁵⁰ Z. G. Xiao,⁵⁷ G. Xie,³¹ W. Xie,⁴⁴ H. Xu,²¹ N. Xu,³¹ Q. H. Xu,⁴⁹ Y. Xu,⁴⁹ Z. Xu,⁶ Z. Xu,⁹
C. Yang,⁴⁹ Q. Yang,⁴⁹ S. Yang,⁴⁵ Y. Yang,³⁷ Z. Ye,⁴⁵ Z. Ye,¹² L. Yi,⁴⁹ K. Yip,⁶ Y. Yu,⁴⁹ H. Zbroszczyk,⁶¹
W. Zha,⁴⁸ C. Zhang,⁵² D. Zhang,¹¹ J. Zhang,⁴⁹ S. Zhang,¹² S. Zhang,¹⁸ X. P. Zhang,⁵⁷ Y. Zhang,²⁶ Y. Zhang,⁴⁸
Y. Zhang,¹¹ Z. J. Zhang,³⁷ Z. Zhang,⁶ Z. Zhang,¹² J. Zhao,⁴⁴ C. Zhou,¹⁸ X. Zhu,⁵⁷ M. Zurek,⁴ and M. Zyzak¹⁷

(STAR Collaboration)

- ¹Abilene Christian University, Abilene, Texas 79699
- ²AGH University of Science and Technology, FPACS, Cracow 30-059, Poland
- ³Alikhanov Institute for Theoretical and Experimental Physics NRC "Kurchatov Institute", Moscow 117218, Russia
- ⁴Argonne National Laboratory, Argonne, Illinois 60439
- ⁵American University of Cairo, New Cairo 11835, New Cairo, Egypt
- ⁶Brookhaven National Laboratory, Upton, New York 11973
- ⁷University of California, Berkeley, California 94720
- ⁸University of California, Davis, California 95616
- ⁹University of California, Los Angeles, California 90095
- ¹⁰University of California, Riverside, California 92521
- ¹¹Central China Normal University, Wuhan, Hubei 430079
- ¹²University of Illinois at Chicago, Chicago, Illinois 60607
- ¹³Creighton University, Omaha, Nebraska 68178
- ¹⁴Czech Technical University in Prague, FNSPE, Prague 115 19, Czech Republic
- ¹⁵Technische Universität Darmstadt, Darmstadt 64289, Germany
- ¹⁶ELTE Eötvös Loránd University, Budapest, Hungary H-1117
- ¹⁷Frankfurt Institute for Advanced Studies FIAS, Frankfurt 60438, Germany
- ¹⁸Fudan University, Shanghai, 200433
- ¹⁹University of Heidelberg, Heidelberg 69120, Germany
- ²⁰University of Houston, Houston, Texas 77204
- ²¹Huzhou University, Huzhou, Zhejiang 313000
- ²²Indian Institute of Science Education and Research (IISER), Berhampur 760010, India
- ²³Indian Institute of Science Education and Research (IISER) Tirupati, Tirupati 517507, India
- ²⁴Indian Institute Technology, Patna, Bihar 801106, India
- ²⁵Indiana University, Bloomington, Indiana 47408
- ²⁶Institute of Modern Physics, Chinese Academy of Sciences, Lanzhou, Gansu 730000
- ²⁷University of Jammu, Jammu 180001, India
- ²⁸Joint Institute for Nuclear Research, Dubna 141 980, Russia
- ²⁹Kent State University, Kent, Ohio 44242
- ³⁰University of Kentucky, Lexington, Kentucky 40506-0055
- ³¹Lawrence Berkeley National Laboratory, Berkeley, California 94720
- ³²Lehigh University, Bethlehem, Pennsylvania 18015
- ³³Max-Planck-Institut für Physik, Munich 80805, Germany
- ³⁴Michigan State University, East Lansing, Michigan 48824
- ³⁵National Research Nuclear University MEPHI, Moscow 115409, Russia
- ³⁶National Institute of Science Education and Research, HBNI, Jatni 752050, India
- ³⁷National Cheng Kung University, Tainan 70101
- ³⁸Nuclear Physics Institute of the CAS, Rez 250 68, Czech Republic
- ³⁹Ohio State University, Columbus, Ohio 43210
- ⁴⁰Institute of Nuclear Physics PAN, Cracow 31-342, Poland
- ⁴¹Panjab University, Chandigarh 160014, India
- ⁴²Pennsylvania State University, University Park, Pennsylvania 16802
- ⁴³NRC "Kurchatov Institute", Institute of High Energy Physics, Protvino 142281, Russia
- ⁴⁴Purdue University, West Lafayette, Indiana 47907
- ⁴⁵Rice University, Houston, Texas 77251
- ⁴⁶Rutgers University, Piscataway, New Jersey 08854
- ⁴⁷Universidade de São Paulo, São Paulo, Brazil 05314-970
- ⁴⁸University of Science and Technology of China, Hefei, Anhui 230026
- ⁴⁹Shandong University, Qingdao, Shandong 266237
- ⁵⁰Shanghai Institute of Applied Physics, Chinese Academy of Sciences, Shanghai 201800
- ⁵¹Southern Connecticut State University, New Haven, Connecticut 06515
- ⁵²State University of New York, Stony Brook, New York 11794
- ⁵³Instituto de Alta Investigación, Universidad de Tarapacá, Arica 1000000, Chile
- ⁵⁴Temple University, Philadelphia, Pennsylvania 19122
- ⁵⁵Texas A&M University, College Station, Texas 77843
- ⁵⁶University of Texas, Austin, Texas 78712
- ⁵⁷Tsinghua University, Beijing 100084
- ⁵⁸University of Tsukuba, Tsukuba, Ibaraki 305-8571, Japan
- ⁵⁹Valparaiso University, Valparaiso, Indiana 46383
- ⁶⁰Variable Energy Cyclotron Centre, Kolkata 700064, India
- ⁶¹Warsaw University of Technology, Warsaw 00-661, Poland
- ⁶²Wayne State University, Detroit, Michigan 48201

⁶³Yale University, New Haven, Connecticut 06520

(Dated: June 10, 2022)

Understanding gluon density distributions and how they are modified in nuclei are among the most important goals in nuclear physics. In recent years, diffractive vector meson production measured in ultra-peripheral collisions (UPCs) at heavy-ion colliders has provided a new tool for probing the gluon density. In this Letter, we report the first measurement of J/ψ photoproduction off the deuteron in UPCs at the center-of-mass energy $\sqrt{s_{NN}} = 200$ GeV in d+Au collisions. The differential cross section as a function of momentum transfer $-t$ is measured. In addition, data with a neutron tagged in the deuteron-going Zero-Degree Calorimeter is investigated for the first time, which is found to be consistent with the expectation of incoherent diffractive scattering at low momentum transfer. Theoretical predictions based on the Color Glass Condensate saturation model and the gluon shadowing model are compared with the data quantitatively. A better agreement with the saturation model has been observed. With the current measurement, the results are found to be directly sensitive to the gluon density distribution of the deuteron and the deuteron breakup, which provides insights into the nuclear gluonic structure.

Keywords: ultra-peripheral collision, vector meson production, deuteron, gluon density distributions

One of the most outstanding problems in modern nuclear physics is the origin of nuclear modifications [1–7]. In the valence quark region, the structure of a bound nucleon in medium and heavy nuclei was found to be significantly different from that of a free nucleon, which is known as the EMC effect [8]. The EMC effect has been a standing puzzle for almost 40 years, while the origin of this modification has not yet been fully understood. Furthermore, the problem of nuclear modification is far more complicated than just the EMC effect, because gluons are also found to be modified in a nuclear environment (See Ref. [9] for a review). In addition to inclusive high energy deep inelastic scattering measurements, an experimental tool for studying the gluon density is the measurement of Vector Meson (VM) photoproduction, e.g., ρ^0 or J/ψ , off nuclear targets [10–23].

In recent analyses carried out by the Large Hadron Collider (LHC) collaborations [15, 16, 18–23], photoproduction of the J/ψ meson has been measured in ultra-peripheral collisions (UPCs) of heavy ions. The resulting cross sections were found to be significantly suppressed with respect to that of a free proton [15, 16, 21, 22]. Leading Twist Approximation (LTA) calculations strongly suggest that the suppression is caused by the gluon shadowing effect [24–26], while other models, e.g., the Color Dipole Model with gluon saturation and nucleon shape fluctuations [27], can also describe the UPC data qualitatively. Similar to the EMC effect, the mechanism of gluon modification in the nuclear environment remains unknown.

An interesting experimental approach to reveal the gluonic structure of nuclei is to study the deuteron - the simplest nuclear bound state of one proton and one neutron. While neither saturation nor gluon shadowing effect is expected to be significant in such loosely bound system, the deuteron may provide unique physics insights in understanding phenomena that are poorly understood from

data of heavy nuclei, e.g., the interplay between coherent and incoherent VM productions, nuclear breakups, single and double nucleon scattering, and short-range nuclear correlations. Recent studies have shown the importance of understanding the parton modifications in light nuclei [28–30], where (gluon) EMC effects and short-range nuclear correlations might be deeply connected. This is a subject of interest for a wide range of physics communities, from nuclear and particle physics to high density neutron stars in astrophysics.

In this Letter, we investigate the differential cross section of J/ψ photoproduction as a function of momentum transfer, $-t$, in d+Au UPC events at $\sqrt{s_{NN}} = 200$ GeV. In the photoproduction limit, the momentum transfer variable $-t$ can be approximated by the transverse momentum squared of J/ψ particles, $p_{T,J/\psi}^2$. The approximate photon-nucleon center-of-mass energy is [31], $W = \sqrt{2\langle E_N \rangle M_{J/\psi} e^{-y}} \sim 25$ GeV, where E_N is the average per nucleon beam energy, $M_{J/\psi}$ is the mass of the J/ψ particle, and y is the J/ψ rapidity. In addition, the differential J/ψ cross section with single neutron tagged events is reported. The data are compared with different theoretical models, where these model predictions are based on an extension of the saturation model and the gluon shadowing model from heavy nuclei to light nuclei [26, 32, 33].¹

The Solenoidal Tracker At RHIC (STAR) detector [34] and its subsystems have been thoroughly described in previous STAR papers [35, 36]. This analysis utilizes several subsystems of the STAR detector. Charged particle tracking, including transverse momentum reconstruction and charge sign determination, is provided by the Time Projection Chamber (TPC) [37] positioned in a 0.5 Tesla longitudinal magnetic field. The TPC volume extends between 50 and 200 cm from the beam axis and covers

¹Both model calculations are made specifically to the d+Au UPC data at RHIC, where Ref. [33] is an extension of Ref. [26] from heavy nuclei at the LHC to the deuteron at RHIC.

* Deceased

pseudorapidities $|\eta| < 1.0$ and over the full azimuthal angle, $0 < \phi < 2\pi$. Surrounding the TPC is the Barrel Electromagnetic Calorimeter (BEMC) [38], which is a lead-scintillator sampling calorimeter. The BEMC is segmented into 4800 optically isolated towers covering the full azimuthal angle for pseudorapidities $|\eta| < 1.0$. There are two Beam-Beam Counters (BBCs) [39], one on each side of the STAR main detector, covering a pseudorapidity range of $3.4 < |\eta| < 5.0$. There are also two ZDCs [34], used to determine and monitor the luminosity and tag the forward neutrons.

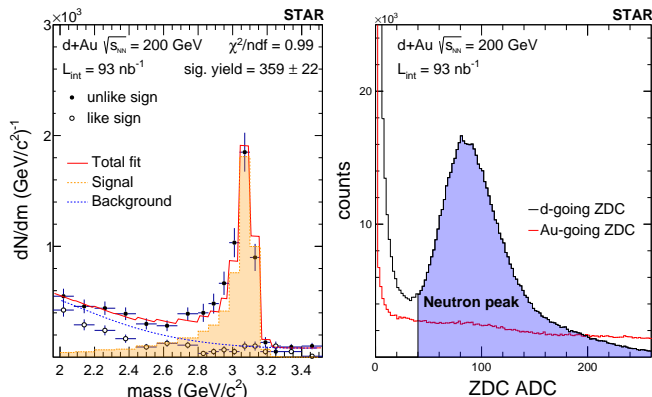


FIG. 1. Left: invariant mass distribution and fit of J/ψ particles photoproduced off the deuteron target at hadronic center-of-mass energy 25 GeV in d+Au ultra-peripheral collisions. Right: Zero-Degree Calorimeter (ZDC) energy deposition (arbitrary units) distribution for both Au- and deuteron-going directions.

The UPC data used for this analysis were collected by the STAR Collaboration during the 2016 d+Au run. The integrated luminosity of the dataset used is approximately 93 nb^{-1} . A total of $\sim 2 \times 10^6$ UPC J/ψ -triggered events are used. The UPC J/ψ trigger is defined by no signal in either BBC East or West, Time-Of-Flight (TOF) [34] track multiplicity between 2 and 6, and a topological selection of back-to-back clusters in the BEMC. In the offline analysis, the events are required to have a valid vertex that is reconstructed within 100 cm of the center of the STAR experiment. In addition, a valid event is required to have at least two TPC tracks associated with the primary vertex with transverse momentum $p_T > 0.5 \text{ GeV}/c$ and $|\eta| < 1.0$. Tracks reconstructed in the TPC are required to have at least 25 space points (out of a maximum of 45) to ensure sufficient momentum resolution, contain no fewer than 15 points for the ionization energy loss (dE/dx) determination to ensure good dE/dx resolution, and to be matched to a BEMC cluster. Furthermore, tracks are required to have a distance of closest approach less than 3 cm to the primary vertex. In order to further select electron candidates, the dE/dx of a charged track is used. The variable $n_{\sigma,e}$ ($n_{\sigma,\pi}$) is the difference between the measured dE/dx value compared to an electron (π) hypothesis of the predicted dE/dx value.

It is calculated in terms of number of standard deviations from the prediction mean. The variable $\chi_{e^+e^-}^2$ is defined as $n_{\sigma,e^+}^2 + n_{\sigma,e^-}^2$ (similar for π). For the region of $\chi_{\pi^+\pi^-}^2 < 30$, the ratio $\chi_{e^+e^-}^2/\chi_{\pi^+\pi^-}^2$ is required to be less than $1/3$, while for $\chi_{\pi^+\pi^-}^2 > 30$, $\chi_{e^+e^-}^2$ must be less than 10. This selection ensures the purity of electrons is higher than 95%, which is determined by a data-driven approach using photonic electrons [35].

The unlike sign electron candidates are paired to reconstruct an invariant mass distribution, while the like sign pairs are also investigated to indicate the contribution from the combinatorial background. The resulting J/ψ candidates are required to have a rapidity $|y| < 1.0$. In Fig. 1 (left), the invariant mass distribution is shown with a template fit to extract the raw yield of J/ψ particles. The signal template is taken from the STARlight [40] Monte Carlo program that was run through the STAR detector GEANT3 simulation [41] for its detector response, indicated by the shaded histogram. Motivated by contributions from the two-photon interaction ($\gamma\gamma \rightarrow e^+e^-$) [42–44] and the combinatorial backgrounds, the background function is taken to be of the form, $(m-A)e^{B(m-A)(m-C)+Cm^3}$, and the fitted result is shown as the dotted line, where m is the invariant mass, A , B , and C are free parameters [31]. The raw yield of the entire analyzed sample after full event selections and background subtraction is 359 ± 22 . For measurement of the differential cross section, raw yields of each $p_{T,J/\psi}^2$ interval are determined based on the same fitting procedure. In Fig. 1 (right), the ZDC energy depositions in terms of Analog-to-Digital Converter (ADC) count are shown for both Au- and deuteron-going directions. For the deuteron-going direction, an ADC count larger than 40 is required for events associated with single neutron emission. Note that after extracting the J/ψ signal, no significant background (pedestal) has been found under the neutron peak for the ADC count larger than 40.

The differential cross section of J/ψ photoproduction as a function of $-t$ is measured in the photon-deuteron system as follows:

$$\frac{d^2\sigma}{dt dy} = \frac{1}{\Phi_{T,\gamma} L_{int} \times BR(ee) \times \Delta t \times \Delta y \times (A \times \epsilon) \times \epsilon_{trig}} N_{obs} \quad (1)$$

Here $\Phi_{T,\gamma} = 11.78$ is the transversely polarized photon flux based on the STARlight MC generator [40], N_{obs} is the raw J/ψ yield, L_{int} is the integrated luminosity, $BR(ee)$ is the branching ratio of J/ψ decaying into electron pair, Δt is the bin width of $p_{T,J/\psi}^2$, $\Delta y = 2.0$ is the rapidity range, $A \times \epsilon$ is the J/ψ reconstruction acceptance and efficiency corrections, and ϵ_{trig} is the trigger efficiency correction. The J/ψ reconstruction efficiency and trigger efficiency correction are based on the STARlight MC events embedded into STAR zero-bias events, where an unfolding technique is employed in the correction procedure. The default unfolding algorithm is based on the Bayesian method from the RooUnfold software package [45].

Different sources of systematic uncertainty on the differential cross section were investigated. Variations of the fit functions, signal templates, yield extraction methods (bin counting vs fit parameter), and momentum resolution of tracks yield a combined systematic uncertainty of 7.3%. Track selections with more than 20 or 30 space points in TPC hits, with more than 10 or 20 space points of dE/dx determination, and less than 2 cm in a distance of closest approach with respect to the primary vertex were investigated and found to lead to a systematic uncertainty of 4%. Variation of the electron identification selection yields a systematic uncertainty of 2%. The systematic uncertainty associated with the unfolding technique, e.g., regularization parameter (4 vs 10 iterations), unfolding algorithm (RooUnfold Bayesian vs TUnfold [46]), and modified underlying truth distributions (exponential vs flat), is found to be 3%. The trigger efficiency associated with the trigger simulation of the BEMC is found to have an uncertainty of 8%. The systematic uncertainty on the integrated luminosity determined by the STAR experiment during this d+Au run is 10% [47, 48]. Finally, the systematic uncertainty on modeling the transversely polarized photon flux is found to be 2% by varying the Au radius of ± 0.5 fm, where a similar study has been done in Ref. [31] at the LHC. The different sources of uncertainty are added in quadrature for the total systematic uncertainty, which is found to be 15.8%. The systematic uncertainty is largely independent of $-t$, which is expected given the daughter electrons in the studied kinematic region are within a range of momentum with good detector resolutions.

In Fig. 2, the fully corrected differential cross section of J/ψ photoproduction in d+Au UPCs at $\sqrt{s_{NN}} = 200$ GeV is shown. The total diffractive J/ψ cross section is labelled “Total data”. Figure. 2 also shows the n -tagged data, which requires that a neutron be detected in the deuteron-going ZDC from deuteron breakup. Note that the cross section of J/ψ photoproduction presented in Fig. 2 can be a mixture of photon-deuteron scattering or photon-gold scattering; however, the probability that the photon is emitted by the deuteron beam is ~ 4 orders of magnitude smaller, therefore negligible in this measurement.

For the full differential cross section reported in this Letter, three distinct physics processes contribute. First, the coherent diffractive process requires that the deuteron stays intact after the interaction. It is possible that the deuteron can be broken up by a secondary soft photon, though this is still considered coherent scattering with regard to the J/ψ production mechanism. The quantitative estimate of the probability of dissociation by a secondary photon is found to be on the order of 0.1% [49, 50], which is not significant to the current measurement. The second contribution is the incoherent diffractive process, where the primary interaction takes place at the nucleon level. Due to the small binding energy of the deuteron (~ 2.2 MeV), the interaction could break the deuteron apart into a proton and a neutron.

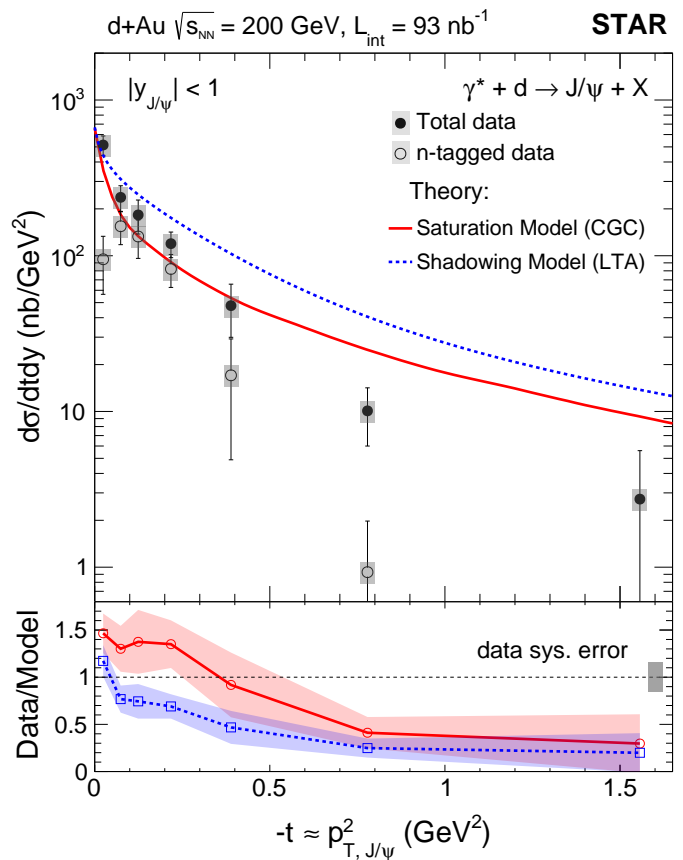


FIG. 2. Upper: differential cross section as a function of $p_{T,J/\psi}^2$ of J/ψ photoproduction in UPCs at $\sqrt{s_{NN}} = 200$ GeV. Data for the total diffractive process are shown with solid markers, while data with neutron tagging in the deuteron-going ZDC are shown with open markers. Theoretical predictions based on the saturation model (Color Glass Condensate) [32] and the gluon shadowing model (LTA) [33] are compared with data, shown as solid lines. Statistical uncertainty is represented by the error bars, and the systematic uncertainty is denoted by the shaded box. For the lower, ratios of total data and models are presented as a function of $-t \approx p_{T,J/\psi}^2$. Color bands are statistical uncertainty based on the data only, while systematic uncertainty is indicated by the gray box.

The last contribution is similar to the second, but the active nucleon fragments and produces particles. When the deuteron is dissociated by either a primary or secondary photon, the spectator nucleon is expected to go in the forward direction.

During the d+Au data taking at STAR, the only forward detector available was the ZDC. The STAR ZDC has approximately ± 2.5 –3 mrad of angular acceptance [51], which corresponds to almost 100% acceptance when the neutron is the spectator nucleon. However, when the neutron is the leading nucleon interacting with the quasi-real photon, the nearly 100% acceptance is only valid for $p_{T,J/\psi}^2 \approx p_{T,neutron}^2 < 0.1$ GeV². Therefore, with the ZDC detector alone, separating the three physics pro-

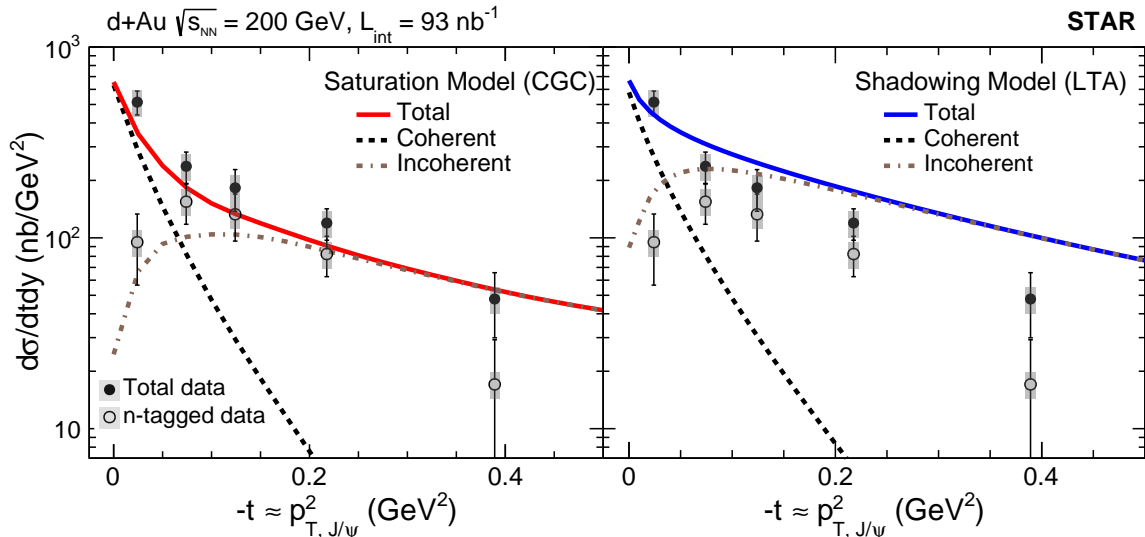


FIG. 3. Theoretical predictions of the saturation model [32] (left) and the gluon shadowing model [33] (right). Coherent and incoherent contributions from the two models are presented separately by dashed lines.

cesses described above across the entire kinematic range is extremely difficult. In the very low $-t$ region, though, the n -tagged events are expected to be dominated by the incoherent scattering process [49, 50], where the ZDC would be able to capture most of the breakup neutrons. In addition, there is the possibility of more complicated incoherent scattering processes, e.g., the photon interacts with both nucleons simultaneously [52–54], where the data with neutron tagging reported in this measurement will be extremely helpful in constraining these scenarios.

In order to further understand the structure of gluons in the deuteron, we compare our data quantitatively with theoretical predictions. There are two major models available to predict the J/ψ photoproduction cross section in UPCs. One is based on the saturation model using a dipole-target scattering formalism [32], while the other is based on the gluon shadowing model using LTA and Impulse Approximation (IA) [33]. It is important to note that for STAR kinematics, where Bjorken- $x \sim 0.01$, a very small saturation or shadowing effect is expected. Without these effects, however, the data and model comparisons (and comparison between models) will be more sensitive to the underlying gluon density distributions, deuteron breakup processes, etc. There are a few model variations available for comparison with the STAR data, while only one variation from each model is presented in Fig. 2. The presented CGC prediction uses a AV18 deuteron wavefunction [55] with Q_s /shape fluctuations [32]. The presented shadowing model uses the LTA formalism. Other model variations and their comparisons to the data are available in the Supplementary Material. In Fig. 2, both models present the sum of all diffractive processes (coherent and incoherent), denoted by the solid lines. The ratios between the total data and

the two models are shown in the lower panel. Note that the theoretical uncertainties related to these two models are significantly less than those of the data in the measured $-t$ range, and therefore are not shown.

It is found that the prediction based on the saturation model describes the data better quantitatively. The data and the saturation model comparison in terms of χ^2 per degree of freedom is found to be 3.38. On the other hand, the gluon shadowing model over predicts the data over most of the measured $-t$ range except for the first bin. The overall data and model comparison in terms of χ^2 per degree of freedom is 13.41, which is significantly larger than that of the saturation model. In these analyses, no model parameters are allowed to vary, and so the absolute differential cross sections from the models are directly compared with the data.

In Fig. 3, our total and n -tagged data are compared with the same model predictions from Fig. 2, but decomposed into coherent and incoherent contributions. For the coherent process, the gluon shadowing model predicts a similar $-t$ distribution as that of the saturation model, where the slope of coherent $-t$ distribution is generally a measure of the target size [56]. In contrast, the incoherent contributions are found to be similar at high $-t$ but significantly different at low $-t$. Both models have been constrained by the HERA electron-proton measurements [57], which leads to similar high $-t$ descriptions. However, the low $-t$ distribution is in a regime that is sensitive to the deuteron breakup, where no experimental data were available prior to this measurement. Therefore, by using the forward neutron tagging in the ZDC, the n -tagged data in Fig. 3 provides the first direct measurement of the incoherent diffractive J/ψ production at low $-t$. The result is found to be in better agreement with the incoherent prediction based on the saturation

model. A quantitative comparison between the n -tagged data and incoherent contributions from the two models can be found in the Supplementary Material.

In conclusion, the differential cross section of J/ψ photoproduction has been measured as a function of momentum transfer $-t$ in d+Au ultra-peripheral collisions at $\sqrt{s_{NN}} = 200$ GeV using the STAR detector. The data are corrected to the photon-deuteron system, where final-state particles from deuteron breakup are all included. In addition, the differential cross section with a single neutron detected in the deuteron-going Zero-Degree Calorimeter is reported. The data are compared with theoretical predictions based on the Color Glass Condensate saturation model and the gluon shadowing model. The data are found to be in better agreement with the saturation model, for both the total diffractive process and the incoherent diffractive process. The data and model comparisons reported in this Letter place significant experimental constraints on the deuteron gluon density distributions and the deuteron breakups. The reported differential cross section of J/ψ photoproduction will become an experimental baseline for a high precision measurement of diffractive J/ψ production at the upcoming Electron-Ion Collider.

We thank the RHIC Operations Group and RCF at

BNL, the NERSC Center at LBNL, and the Open Science Grid consortium for providing resources and support. This work was supported in part by the Office of Nuclear Physics within the U.S. DOE Office of Science, the U.S. National Science Foundation, the Ministry of Education and Science of the Russian Federation, National Natural Science Foundation of China, Chinese Academy of Science, the Ministry of Science and Technology of China and the Chinese Ministry of Education, the Higher Education Sprout Project by Ministry of Education at NCKU, the National Research Foundation of Korea, Czech Science Foundation and Ministry of Education, Youth and Sports of the Czech Republic, Hungarian National Research, Development and Innovation Office, New National Excellency Programme of the Hungarian Ministry of Human Capacities, Department of Atomic Energy and Department of Science and Technology of the Government of India, the National Science Centre of Poland, the Ministry of Science, Education and Sports of the Republic of Croatia, RosAtom of Russia and German Bundesministerium für Bildung, Wissenschaft, Forschung und Technologie (BMBF), Helmholtz Association, Ministry of Education, Culture, Sports, Science, and Technology (MEXT) and Japan Society for the Promotion of Science (JSPS).

-
- [1] J. Aubert *et al.* (European Muon), The ratio of the nucleon structure functions $F2_n$ for iron and deuterium, Phys. Lett. B **123**, 275 (1983).
- [2] J. Ashman *et al.* (European Muon), Measurement of the Ratios of Deep Inelastic Muon - Nucleus Cross-Sections on Various Nuclei Compared to Deuterium, Phys. Lett. B **202**, 603 (1988).
- [3] J. Gomez *et al.*, Measurement of the A-dependence of deep inelastic electron scattering, Phys. Rev. D **49**, 4348 (1994).
- [4] M. Arneodo *et al.* (European Muon), Shadowing in Deep Inelastic Muon Scattering from Nuclear Targets, Phys. Lett. B **211**, 493 (1988).
- [5] M. Arneodo *et al.* (European Muon), Measurements of the nucleon structure function in the range $0.002 - \text{GeV}^2 < x < 0.17 - \text{GeV}^2$ and $0.2 - \text{GeV}^2 < q^2 < 8 - \text{GeV}^2$ in deuterium, carbon and calcium, Nucl. Phys. B **333**, 1 (1990).
- [6] D. Allasia *et al.* (New Muon (NMC)), Measurement of the neutron and the proton F2 structure function ratio, Phys. Lett. B **249**, 366 (1990).
- [7] J. Seely *et al.*, New measurements of the EMC effect in very light nuclei, Phys. Rev. Lett. **103**, 202301 (2009), arXiv:0904.4448 [nucl-ex].
- [8] T. Sloan, *History of the European Muon Collaboration (EMC)*, Vol. 5/2019 (2019).
- [9] A. Accardi *et al.*, Electron Ion Collider: The Next QCD Frontier, Eur. Phys. J. **A52**, 268 (2016), arXiv:1212.1701 [nucl-ex].
- [10] T. Nash, A. Belousov, B. Govorkov, D. O. Caldwell, J. P. Cumalat, A. M. Eisner, R. J. Morrison, F. V. Murphy, S. J. Yellin, P. J. Davis, R. M. Eglhoff, G. Luste, and J. D. Prentice, Measurement of $\frac{J}{\psi}(3100)$ photoproduction in deuterium at a mean energy of 55 gev, Phys. Rev. Lett. **36**, 1233 (1976).
- [11] M. Binkley, C. Bohler, J. Butler, J. Cumalat, I. Gaines, M. Gormley, D. Harding, R. L. Loveless, J. Peoples, P. Callahan, G. Gladding, C. Olszewski, and A. Wattenberg, $\frac{J}{\psi}$ photoproduction from 60 to 300 gev/c, Phys. Rev. Lett. **48**, 73 (1982).
- [12] M. Arneodo *et al.* (New Muon), Quasielastic J / psi muoproduction from hydrogen, deuterium, carbon and tin, Phys. Lett. B **332**, 195 (1994).
- [13] C. Adler *et al.* (STAR), Coherent rho0 production in ultraperipheral heavy ion collisions, Phys. Rev. Lett. **89**, 272302 (2002), arXiv:nucl-ex/0206004.
- [14] S. L. Timoshenko (STAR), rho meson production in ultraperipheral dAu collision, in *17th International Baldin Seminar on High Energy Physics Problems: Relativistic Nuclear Physics and Quantum Chromodynamics*, Vol. V1 (2005) pp. 292–295, arXiv:nucl-ex/0501010.
- [15] V. Khachatryan *et al.* (CMS), Coherent J/ψ photoproduction in ultra-peripheral PbPb collisions at $\sqrt{s_{NN}} = 2.76$ TeV with the CMS experiment, Phys. Lett. B **772**, 489 (2017), arXiv:1605.06966 [nucl-ex].
- [16] B. Abelev *et al.* (ALICE), Coherent J/ψ photoproduction in ultra-peripheral Pb-Pb collisions at $\sqrt{s_{NN}} = 2.76$ TeV, Phys. Lett. B **718**, 1273 (2013), arXiv:1209.3715 [nucl-ex].
- [17] J. Adam *et al.* (ALICE), Coherent ρ^0 photoproduction in ultra-peripheral Pb-Pb collisions at $\sqrt{s_{NN}} = 2.76$ TeV, JHEP **09**, 095, arXiv:1503.09177 [nucl-ex].
- [18] L. Adamczyk *et al.* (STAR), Coherent diffractive photoproduction of ρ^0 mesons on gold nuclei at 200

- GeV/nucleon-pair at the Relativistic Heavy Ion Collider, Phys. Rev. C **96**, 054904 (2017), arXiv:1702.07705 [nucl-ex].
- [19] S. Acharya *et al.* (ALICE), Coherent photoproduction of ρ^0 vector mesons in ultra-peripheral Pb-Pb collisions at $\sqrt{s_{NN}} = 5.02$ TeV, JHEP **06**, 035, arXiv:2002.10897 [nucl-ex].
- [20] S. Acharya *et al.* (ALICE), First measurement of coherent ρ^0 photoproduction in ultra-peripheral Xe-Xe collisions at $\sqrt{s_{NN}} = 5.44$ TeV, (2021), arXiv:2101.02581 [nucl-ex].
- [21] S. Acharya *et al.* (ALICE), First measurement of the $|t|$ -dependence of coherent J/ψ photonuclear production, (2021), arXiv:2101.04623 [nucl-ex].
- [22] S. Acharya *et al.* (ALICE), Coherent J/ψ and ψ' photoproduction at midrapidity in ultra-peripheral Pb-Pb collisions at $\sqrt{s_{NN}} = 5.02$ TeV, (2021), arXiv:2101.04577 [nucl-ex].
- [23] R. Aaij *et al.* (LHCb), Study of J/ψ photo-production in lead-lead peripheral collisions at $\sqrt{s_{NN}} = 5$ TeV, (2021), arXiv:2108.02681 [hep-ex].
- [24] M. Alvioli, L. Frankfurt, V. Guzey, M. Strikman, and M. Zhalov, Color fluctuation phenomena in γA collisions at the LHC, CERN Proc. **1**, 151 (2018).
- [25] V. Guzey and M. Zhalov, Exclusive J/ψ production in ultraperipheral collisions at the LHC: constrains on the gluon distributions in the proton and nuclei, JHEP **10**, 207, arXiv:1307.4526 [hep-ph].
- [26] V. Guzey, M. Strikman, and M. Zhalov, Nucleon dissociation and incoherent J/ψ photoproduction on nuclei in ion ultraperipheral collisions at the Large Hadron Collider, Phys. Rev. C **99**, 015201 (2019), arXiv:1808.00740 [hep-ph].
- [27] B. Sambasivam, T. Toll, and T. Ullrich, Investigating saturation effects in ultraperipheral collisions at the LHC with the color dipole model, Phys. Lett. B **803**, 135277 (2020), arXiv:1910.02899 [hep-ph].
- [28] Z. Tu, A. Jentsch, M. Baker, L. Zheng, J.-H. Lee, R. Venugopalan, O. Hen, D. Higinbotham, E.-C. Aschenauer, and T. Ullrich, Probing short-range correlations in the deuteron via incoherent diffractive J/ψ production with spectator tagging at the EIC, Phys. Lett. B **811**, 135877 (2020), arXiv:2005.14706 [nucl-ex].
- [29] W. Cosyn and C. Weiss, Polarized electron-deuteron deep-inelastic scattering with spectator nucleon tagging, Phys. Rev. C **102**, 065204 (2020), arXiv:2006.03033 [hep-ph].
- [30] M. Strikman and C. Weiss, Electron-deuteron deep-inelastic scattering with spectator nucleon tagging and final-state interactions at intermediate x , Phys. Rev. C **97**, 035209 (2018), arXiv:1706.02244 [hep-ph].
- [31] B. B. Abelev *et al.* (ALICE), Exclusive J/ψ photoproduction off protons in ultra-peripheral p-Pb collisions at $\sqrt{s_{NN}} = 5.02$ TeV, Phys. Rev. Lett. **113**, 232504 (2014), arXiv:1406.7819 [nucl-ex].
- [32] H. Mäntysaari and B. Schenke, Accessing the gluonic structure of light nuclei at a future electron-ion collider, Phys. Rev. C **101**, 015203 (2020), arXiv:1910.03297 [hep-ph].
- [33] V. Guzey, M. Strikman, E. Kryshen, and M. Zhalov, LTA predictions for J/ψ photoproduction in d+Au UPCs at RHIC (2021).
- [34] K. H. Ackermann *et al.* (STAR), STAR detector overview, Nucl. Instrum. Meth. A **499**, 624 (2003).
- [35] J. Adam *et al.* (STAR), Low- p_T e^+e^- pair production in Au+Au collisions at $\sqrt{s_{NN}} = 200$ GeV and U+U collisions at $\sqrt{s_{NN}} = 193$ GeV at STAR, Phys. Rev. Lett. **121**, 132301 (2018), arXiv:1806.02295 [hep-ex].
- [36] J. Adam *et al.* (STAR), Measurements of W and Z/γ^* cross sections and their ratios in p+p collisions at RHIC, Phys. Rev. D **103**, 012001 (2021), arXiv:2011.04708 [nucl-ex].
- [37] M. Anderson *et al.*, The Star time projection chamber: A Unique tool for studying high multiplicity events at RHIC, Nucl. Instrum. Meth. A **499**, 659 (2003), arXiv:nucl-ex/0301015.
- [38] M. Beddo *et al.* (STAR), The STAR barrel electromagnetic calorimeter, Nucl. Instrum. Meth. A **499**, 725 (2003).
- [39] C. A. Whitten (STAR), The beam-beam counter: A local polarimeter at STAR, AIP Conf. Proc. **980**, 390 (2008).
- [40] S. R. Klein, J. Nystrand, J. Seger, Y. Gorbunov, and J. Butterworth, STARlight: A Monte Carlo simulation program for ultra-peripheral collisions of relativistic ions, Comput. Phys. Commun. **212**, 258 (2017), arXiv:1607.03838 [hep-ph].
- [41] R. Brun, F. Bruyant, M. Maire, A. C. McPherson, and P. Zancarini, GEANT3, <https://cds.cern.ch/record/1119728> (1987).
- [42] J. Adam *et al.* (STAR), Measurement of e^+e^- Momentum and Angular Distributions from Linearly Polarized Photon Collisions, Phys. Rev. Lett. **127**, 052302 (2021), arXiv:1910.12400 [nucl-ex].
- [43] B. Abelev *et al.* (ALICE), Coherent J/ψ photoproduction in ultra-peripheral Pb-Pb collisions at $\sqrt{s_{NN}} = 2.76$ TeV, Phys. Lett. B **718**, 1273 (2013), arXiv:1209.3715 [nucl-ex].
- [44] E. Abbas *et al.* (ALICE), Charmonium and e^+e^- pair photoproduction at mid-rapidity in ultra-peripheral Pb-Pb collisions at $\sqrt{s_{NN}}=2.76$ TeV, Eur. Phys. J. C **73**, 2617 (2013), arXiv:1305.1467 [nucl-ex].
- [45] H. B. Prosper and L. Lyons, eds., *Proceedings, PHYSTAT 2011 Workshop on Statistical Issues Related to Discovery Claims in Search Experiments and Unfolding, CERN, Geneva, Switzerland 17-20 January 2011*, CERN Yellow Reports: Conference Proceedings (CERN, Geneva, 2011).
- [46] S. Schmitt, TUnfold: an algorithm for correcting migration effects in high energy physics, JINST **7**, T10003, arXiv:1205.6201 [physics.data-an].
- [47] B. I. Abelev *et al.* (STAR), Rapidity and species dependence of particle production at large transverse momentum for d+Au collisions at $s(NN)^{(1/2)} = 200$ -GeV, Phys. Rev. C **76**, 054903 (2007), arXiv:nucl-ex/0609021.
- [48] J. Adams *et al.* (STAR), Evidence from d + Au measurements for final state suppression of high p(T) hadrons in Au+Au collisions at RHIC, Phys. Rev. Lett. **91**, 072304 (2003), arXiv:nucl-ex/0306024.
- [49] S. Klein and R. Vogt, Deuteron photodissociation in ultraperipheral relativistic heavy ion on deuteron collisions, Phys. Rev. C **68**, 017902 (2003), arXiv:nucl-ex/0303013.
- [50] A. J. Baltz, S. R. Klein, and J. Nystrand, Coherent vector meson photoproduction with nuclear breakup in relativistic heavy ion collisions, Phys. Rev. Lett. **89**, 012301 (2002), arXiv:nucl-th/0205031.
- [51] J. Adams *et al.* (STAR), Pseudorapidity asymmetry and centrality dependence of charged hadron spectra in d + Au collisions at $S(NN)^{(1/2)} = 200$ -GeV, Phys. Rev. C

- 70**, 064907 (2004), arXiv:nucl-ex/0408016.
- [52] T. H. Bauer, R. D. Spital, D. R. Yennie, and F. M. Pipkin, The hadronic properties of the photon in high-energy interactions, *Rev. Mod. Phys.* **50**, 261 (1978).
- [53] T. H. Bauer, R. D. Spital, D. R. Yennie, and F. M. Pipkin, Erratum: The hadronic properties of the photon in highenergy interactions, *Rev. Mod. Phys.* **51**, 407 (1979).
- [54] T. C. Rogers, M. M. Sargsian, and M. I. Strikman, Coherent vector meson photo-production from deuterium at intermediate energies, *Phys. Rev. C* **73**, 045202 (2006), arXiv:hep-ph/0509101.
- [55] R. B. Wiringa, V. Stoks, and R. Schiavilla, An Accurate nucleon-nucleon potential with charge independence breaking, *Phys. Rev. C* **51**, 38 (1995), arXiv:nucl-th/9408016.
- [56] T. Toll and T. Ullrich, Exclusive diffractive processes in electron-ion collisions, *Phys. Rev. C* **87**, 024913 (2013), arXiv:1211.3048 [hep-ph].
- [57] C. Alexa *et al.* (H1), Elastic and Proton-Dissociative Photoproduction of J/ψ Mesons at HERA, *Eur. Phys. J. C* **73**, 2466 (2013), arXiv:1304.5162 [hep-ex].
- [58] M. L. Miller, K. Reygers, S. J. Sanders, and P. Steinberg, Glauber modeling in high energy nuclear collisions, *Ann. Rev. Nucl. Part. Sci.* **57**, 205 (2007), arXiv:nucl-ex/0701025.

SUPPLEMENTAL MATERIAL

In Table. I, the data and model comparisons are performed based on the Color Glass Condensate saturation model [32] in terms of the χ^2 per degree of freedom, denoted as χ^2/ndf . Different theoretical variations are performed, where the coherent contributions are based on two different deuteron wavefunctions, Hulthen [58] and AV18 [55]. For the incoherent contribution, the authors of Ref. [32] has compared with and without saturation scale (Q_s) and nucleon shape fluctuations. A total of four combinations are presented. Note the fits have no free parameter, therefore the χ^2/ndf values reflect the direct comparisons between data and models. The fit range is between 0 and 1.2 GeV².

It is found that the data slightly favors the AV18 wave functions. However, the two wave functions are very similar at low momentum transfer $-t$ region. For details, see Ref. [32]. In order to distinguish the details of the two wavefunctions, we would need a significant better precision at high $-t$ in the measurement. For the incoherent production, it is mostly sensitive to the high $-t$ region, therefore the data cannot conclude which one is better. Currently, the data is found to be consistent with both scenarios.

TABLE I. It summarizes the goodness of fits in terms of χ^2/ndf between data and theoretical predictions based on the Color Glass Condensate saturation model in different combinations of templates [32].

Data/Model comparisons (coh,incoh)	Goodness of fits χ^2/ndf
(Hulthen, Q_s /shape fluc.)	4.04
(Hulthen, No fluc.)	2.27
(AV18, Q_s /shape fluc.)	3.83
(AV18, No fluc.)	2.09

Similarly, in Table. II, the data are compared with models based on gluon shadowing model with Leading Twist Approximation (LTA) and the Impulse Approxi-

mation (IA) in terms of the χ^2 per degree of freedom [33]. The two comparisons are found to be very similar.

TABLE II. It summarizes the χ^2/ndf between data and theoretical predictions based on gluon shadowing model LTA and the impulse approximation.

Data/Model comparisons	Goodness of fits χ^2/ndf
Impulse Approximation	13.97
Leading Twist Approximation	13.41

Finally, we make comparisons of incoherent predictions from both the saturation model and the gluon shadowing model to the n -tagged data only. As the acceptance of the ZDC is limited, we only compare the data up to 0.3 GeV². The data is found to be quantitatively better described by the saturation model. Given only very small number of available bins (small number of degree of freedom) at low $-t$, the interpretation of the absolute χ^2/ndf values is not meaningful, as some values are significantly below unity. The small number of degrees of freedoms would not reflect the statistical fluctuations. However, to compare which model describes the data is better, the relative difference between the χ^2/ndf values is still reliable.

TABLE III. It summarizes the goodness of fits in terms of χ^2/ndf between data and theoretical predictions based on the saturation model and gluon shadowing model with incoherent production only to the n -tagged data.

Data/Model comparisons	Goodness of fits χ^2/ndf
Saturation - Q_s /shape fluc.	0.81
Saturation - no Q_s /shape fluc.	0.54
Shadowing - LTA	8.38
Shadowing - IA	9.04